Health Environ, 2026, 7(1): 328-344
DOI: 10.25082/HE.2026.01.004

RESEARCH ARTICLE

Green Synthesis of SnO_2/Bentonite Nanocomposite Using *Murraya koenigii* Leaf Extract for Photocatalytic Degradation of Rhodamine B Dye and Carbofuran Pesticide in Aqueous Solution

Samar Jahan[1] **Raziya Nadeem**[1] **Noor Zulfiqar**[1*]

[1] Department of Chemistry, Faculty of Science, University of Agriculture, Faisalabad, Pakistan

Correspondence to: Noor Zulfiqar, Department of Chemistry, Faculty of Science, University of Agriculture, Faisalabad, Pakistan;
E-mail: evunain@unima.ac.mw

Received: June 9, 2026;
Accepted: August 14, 2026;
Published: August 19, 2026.

Citation: Jahan S, Nadeem R, Zulfiqar N. Green Synthesis of SnO_2/Bentonite Nanocomposite Using *Murraya koenigii* Leaf Extract for Photocatalytic Degradation of Rhodamine B Dye and Carbofuran Pesticide in Aqueous Solution. *Health Environ*, 2026, **6**(1): 328-344. https://doi.org/10.25082/HE.2026.01.004

Abstract: Water contamination by synthetic dyes and pesticides is a major environmental concern because of their persistence, toxicity, and adverse effects on aquatic ecosystems and human health. The present study focused on the green synthesis of SnO_2 nanoparticles and the preparation of a SnO_2/bentonite nanocomposite (SBT-NC) using *Murraya koenigii* leaf extract and its application for the photocatalytic degradation of Rhodamine B (RhB) dye and Carbofuran (CBF) pesticide in aqueous solutions. Bentonite was used as a supporting material to improve the adsorption capacity, surface area, and dispersion of SnO_2 nanoparticles. The synthesized materials were characterized using UV–visible spectroscopy, scanning electron microscopy (SEM), energy-dispersive X-ray spectroscopy (EDX), and Fourier-transform infrared spectroscopy (FTIR). The characterization results confirmed the successful formation and incorporation of SnO_2 nanoparticles onto the bentonite matrix. The effects of important experimental parameters, including solution pH, initial pollutant concentration, contact time, and catalyst dosage, were investigated under light irradiation. The SBT-NC showed considerably higher photocatalytic degradation efficiency than pure bentonite and SnO_2 nanoparticles. Under optimized conditions, the degradation efficiency of Rhodamine B reached approximately 92–94%, while Carbofuran degradation reached approximately 90–91%. The optimum conditions included alkaline pH for Rhodamine B and acidic pH for Carbofuran, with a catalyst dosage of approximately 0.1 g and a reaction time of about 90–120 min. The enhanced performance of SBT-NC was attributed to the synergistic effect of the adsorption properties of bentonite and the photocatalytic activity of SnO_2, which provided additional active sites and promoted the formation of reactive oxygen species. Kinetic analysis indicated that the degradation of both pollutants was generally better described by the pseudo-first-order kinetic model. Overall, the green-synthesized SnO_2/bentonite nanocomposite demonstrated strong potential as an efficient, economical, and environmentally friendly photocatalyst for the removal of organic pollutants from contaminated water.

Keywords: SnO_2/bentonite nanocomposite, green synthesis, *Murraya koenigii*, photocatalytic degradation, Wastewater treatment, SnO_2 nanoparticles, organic pollutants, advanced oxidation process

1 Introduction

Freshwater resources are essential for sustaining life and supporting agricultural, industrial, and domestic activities. However, rapid population growth, urbanization, and industrial expansion have resulted in severe deterioration of water quality worldwide. Increasing water demand has accelerated wastewater generation, introducing a wide range of contaminants into aquatic systems. Among various pollutants, organic compounds such as synthetic dyes, pesticides, pharmaceutical residues, and industrial chemicals are considered highly hazardous due to their persistence, toxicity, and potential bioaccumulation. The discharge of these pollutants into water bodies not only reduces water quality but also threatens aquatic ecosystems and human health.

Water pollution caused by industrial and agricultural activities has become a global environmental challenge. Organic contaminants released from textile, pharmaceutical, chemical, agricultural, and food-processing industries can enter surface and groundwater systems through untreated or insufficiently treated wastewater. Exposure to these toxic compounds through

contaminated water and food may cause adverse effects on vital biological systems, including neurological, respiratory, cardiovascular, and digestive systems. Therefore, the development of efficient, sustainable, and cost-effective technologies for wastewater remediation has become an urgent research priority [1–3].

Among organic pollutants, synthetic dyes represent a major class of contaminants due to their extensive application in textile, paper, plastic, printing, pharmaceutical, and food industries. More than 100,000 tons of dyes are produced annually, and a significant proportion is released into the environment through industrial effluents. These colored compounds reduce light penetration in water, disturb photosynthetic processes, and may generate toxic intermediates during degradation. Rhodamine B (RhB), a cationic xanthene dye, is widely used in textile industries, biological staining, analytical chemistry, and as a fluorescent tracer. Despite its industrial importance, Rhodamine B exhibits considerable environmental toxicity and has been associated with carcinogenic and harmful effects on living organisms. Therefore, effective removal of Rhodamine B from contaminated water is necessary before wastewater discharge [4, 5]. (see Table 1)

Table 1 Photocatalysts used for sequestrating dyes

Photocatalysts	**Removal of Dyes**	**Ref.**
SnO2/LaFeO3-$_X$N$_X$ composite	Rhodamine B (RhB) dye	[6]
Au-Ag NPs-decorated TiO_2-modified Fe3O4 composite	Rhodamine-6G (Rh6G)	[7]
Nanocomposite based on ZnS/ChPA (Zinc Sulfide/Chitosan-g-polyacrylamide)	Dyes i.e. Congo Red and Methyl Orange	[8]
Heterojuction porous composites (g-C3N4/SnO2/SiO2)(DOP-CSiSn)	Methyl orange, methylene blue and Rhodamine B	[9]
biogenic SnO2 nanoparticles	Reactive Yellow 186 (RY186)	[10]
Yb2(MoO4)3/YbMoO4 nanocomposite	Methyl Orange, Rhodamine B and Methylene Blue	[11]
Nanocomposite based on Zr(IV) phosphate- Gelatin (ZPNC/GT)	Fast Green, Methylene Blue Dyes	[12]
Nanocomposites based on reduced graphene oxide/β-Tin Tungstate (rGO/β-$SnWO_4$).	Rhodamine B(Rh B) and Methylene Orange (MO)	[13]
microspheres of BiOBr modified with sepiolite and polyvinyl pyrrolidone (PVP)	Rhodamine B	[14]
Cu_2O/rGO nanocomposites	Rhodamine B	[15]
Magnetic AC/CeO2 Nanocomposite	Rhodamine B	[16]
Chitosan-SnO_2 nanocomposites	Azo Dyes	[5]
Co_3O_4/ZnO nanocomposite	Methylene Blue and Rhodamine B	[17]
graphene/zirconium oxide nanocomposite	Rhodamine B dye	[18]
CNF-AgNPs aerogel nanocomposite	Rhodamine B	[19]
Carbon nanotube–cobalt ferrite Nanocomposites	Rhodamine B	[20]
Exfoliated bentonite, g-C_3N_4 and Ag_3PO_4 (EB/gC_3N_4/Ag_3PO_4)nanocomposite	Rhodamine B	[21]
CdS/EP nanocomposites	Rhodamine B	[22]
$Bi_2O_2CO_3$/Bi_2O_4 photocatalyst	Dyes	[23]
Sr/Ce/activated carbon bimetallic nanocomposite	Rhodamine B	[24]
$BaWO_4$ nanoparticles	Rhodamine B	[25]
zinc oxide loaded activated carbon	Orange G and Rhodamine B	[5]
L-Serine capped magnetite nanoparticles	Rhodamine B	[26]
$Co_{1-x}Cu_xFe_2O_4$ ($0 \leq$ x $\leq$ 0.5) nanoparticles	Rhodamine B	[23]
Metallic nanoparticles as a support on $InVO_4$–$BiVO_4$_3DOM	MB and RhB dyes	[27]
Hybrid materials based on reduced graphene oxide (rGO/ Cu_2SnS_3)	Rhodamine B	[28]
Bi_2S_3/BSO composite	Rhodamine B	[29]
Sn0.215In0.38S/reduced graphene oxide composite	high-chroma Rhodamine	[30]
SnS2 nanostructure	Rhodamine B	[31]
SnS nanoparticles	Methylene blue and Rhodamine B.	[32]
2D SnS2/g-C3N4 Z-scheme composite	Rhodamine B (RhB)	[33]
Mesoporous silica (SBA-15) embedded inside SnxTi(1-x)O_2	Rhodamine B	[34]

Besides dyes, pesticides are another important group of emerging aquatic pollutants. Excessive application of synthetic pesticides in agricultural practices has resulted in their widespread occurrence in soil, surface water, and groundwater. Due to their chemical stability and biological toxicity, pesticide residues pose significant risks to ecosystems and human health [35]. Carbofuran, a highly toxic N-methyl carbamate pesticide, has been extensively used for controlling insects and nematodes. Although it can undergo hydrolysis under environmental conditions, its high mobility and widespread application contribute to its persistence in aquatic environments. Carbofuran toxicity is mainly associated with acetylcholinesterase inhibition, leading to neurological disorders and potential fatal outcomes after acute exposure. Consequently, the removal of carbofuran from wastewater is essential for environmental protection.

Several conventional wastewater treatment approaches, including adsorption, coagulation-flocculation, filtration, biological treatment, chlorination, and ozonation, have been applied for pollutant removal. However, these techniques often suffer from limitations such as incomplete degradation, generation of secondary pollutants, high operational costs, and poor efficiency toward chemically stable organic contaminants. Biological treatment methods are generally ineffective for persistent dyes and pesticides due to their complex molecular structures and resistance to biodegradation. Therefore, advanced oxidation processes (AOPs), particularly photocatalytic degradation, have attracted considerable attention as promising strategies for complete mineralization of organic pollutants into harmless products such as carbon dioxide, water, and inorganic ions.

Photocatalysis is an efficient advanced oxidation technology based on the generation of highly reactive oxidative species under light irradiation. Semiconductor photocatalysts produce electron–hole pairs after photon absorption, which subsequently participate in redox reactions to generate reactive oxygen species (ROS), including hydroxyl radicals (•OH) and superoxide radicals ($O_2^{\bullet-}$) [36–38]. These reactive species can effectively degrade complex organic molecules. However, the practical application of many semiconductor photocatalysts is limited by low surface area, electron–hole recombination, and poor stability. Therefore, the development of efficient photocatalytic materials with enhanced surface properties and improved charge separation is required. (see Figure 1)

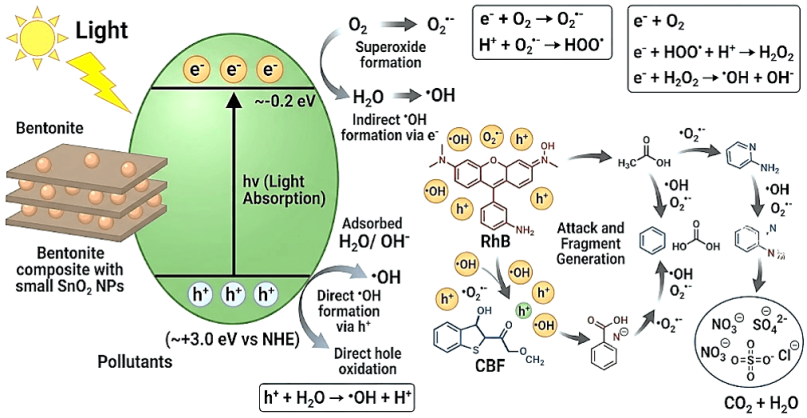

Figure 1 General review of photocatalytic mechanism and degradation process

$$\text{SBT-NC} + h\nu \rightarrow h^+ + e^- \quad (1)$$

$$H_2O + h^+ \rightarrow OH^\bullet + H^+ \quad (2)$$

$$OH^- + h^+ \rightarrow OH^\bullet \quad (3)$$

$$e^- + O_2 \rightarrow O_2^{\bullet-} \quad (4)$$

$$\text{Organic pollutants} + h\nu \rightarrow \text{organic pollutants}^* \quad (5)$$

$$\text{SBT-NC} + \text{organic pollutants}^* \rightarrow \text{SBT-NC}(e^-) + \text{organic pollutants}^+ \quad (6)$$

$$\text{SBT-NC}(e^-) + O_2 \rightarrow \text{SBT-NC} + O_2^- \quad (7)$$

$$2\,\text{SBT-NC}(e^-) + O_2^{\bullet-} + 2H^+ \rightarrow 2\,\text{SBT-NC} + H_2O_2 \quad (8)$$

$$\text{SBT-NC}(e^-) + H_2O_2 \rightarrow \text{SBT-NC} + OH^\cdot + OH^- \quad (9)$$

$$\text{Organic pollutants} + h^+ \rightarrow \text{degradation products} \quad (10)$$

$$\text{Organic pollutants}^* + OH^\cdot/O_2/O_2^{\bullet-} \rightarrow \text{degradation products} \quad (11)$$

Nanotechnology has provided new opportunities for environmental remediation due to the unique physicochemical properties of nanomaterials, including high surface area, tunable electronic structure, and enhanced catalytic activity. Among various semiconductor nanomaterials, tin oxide (SnO_2) has received considerable attention because of its excellent chemical stability, optical transparency, thermal resistance, and suitable electronic properties. SnO_2 nanoparticles can generate electron–hole pairs under irradiation, enabling the formation of reactive oxygen species responsible for pollutant degradation. However, aggregation of nanoparticles and limited adsorption capacity often restrict their practical efficiency.

To overcome these limitations, incorporation of semiconductor nanoparticles onto suitable support materials has emerged as an effective approach. Natural clay minerals, particularly bentonite, have gained significant interest as catalyst supports due to their abundance, low cost, environmental compatibility, high surface area, and excellent adsorption capability. Bentonite, mainly composed of montmorillonite, possesses layered structures with negatively charged surfaces that facilitate adsorption of pollutants and provide favorable environments for nanoparticle dispersion. The combination of SnO_2 nanoparticles with bentonite can therefore improve photocatalytic performance by increasing active surface sites, enhancing pollutant adsorption, and reducing nanoparticle aggregation.

Furthermore, green synthesis approaches have recently gained attention as sustainable alternatives to conventional nanoparticle fabrication methods. Biological synthesis using plant extracts provides environmentally friendly, economical, and non-toxic routes for nanoparticle production by utilizing naturally occurring phytochemicals as reducing and stabilizing agents. *Murraya koenigii* (curry leaf) extract contains bioactive compounds such as carbazoles, flavonoids, and antioxidants, which can contribute to the formation and stabilization of metal oxide nanoparticles [39, 40].

In this study, a green-synthesized SnO_2/bentonite nanocomposite was developed and investigated for the photocatalytic degradation of Rhodamine B dye and Carbofuran pesticide in aqueous solution. The combination of SnO_2 semiconductor properties, bentonite adsorption capability, and environmentally sustainable synthesis strategy provides a promising approach for efficient wastewater treatment. The photocatalytic activity, pollutant degradation efficiency, and underlying degradation mechanism were systematically evaluated to demonstrate the potential application of the prepared nanocomposite for environmental remediation [41–56].

2 Materials and Methods

2.1 Green synthesis of SnO_2 nanoparticles

The green synthesis of SnO_2 nanoparticles was carried out using *Murraya koenigii* leaf extract as a reducing and capping agent. All experiments were conducted in the Analytical Method Development Research Group Laboratory, Department of Chemistry, University of Agriculture, Faisalabad. Fresh *Murraya koenigii* leaves were collected and thoroughly washed with tap water to remove dust and other adhering impurities, followed by washing with distilled water to eliminate residual contaminants. The washed leaves were dried under shade and subsequently ground using a pestle and mortar to obtain fine biomass. A total of 20 g of the dried and powdered leaf biomass was weighed using an electronic balance and mixed with 200 mL of distilled water. The mixture was heated at boiling temperature for 30 min. After cooling to room temperature, the extract was filtered through filter paper and subsequently centrifuged at 6000 rpm to remove suspended particulate matter. The resulting *Murraya koenigii* leaf extract was stored under refrigerated conditions until further use. The prepared leaf extract is shown in Figure 2b.

For the synthesis of SnO_2 nanoparticles, 100 mL of the prepared leaf extract was added dropwise to 50 mL of 0.05 M tin chloride pentahydrate ($SnCl_2{\cdot}5H_2O$) solution under constant magnetic stirring at room temperature for 30 min. A gradual color change from white to light brown was observed during the reaction, indicating the formation of the precursor material. Subsequently, sodium hydroxide solution was added at 60 °C under vigorous stirring until the pH reached 11–12. The reaction mixture was then continuously stirred for 5 h to facilitate nanoparticle formation.

The resulting light-brown precipitates were collected by centrifugation at 4000 rpm and filtered using Whatman filter paper. The precipitates were washed several times with distilled water to remove unreacted and soluble impurities and were subsequently dried at 80 °C for 48 h. The dried material was finally calcined in a muffle furnace at 600 °C for 2 h to obtain the

biosynthesized SnO_2 nanoparticles.

2.2 Preparation of SnO_2/bentonite nanocomposite

The SnO_2/bentonite nanocomposite (SBT-NC) was prepared by incorporating SnO_2 onto bentonite clay through the same green synthesis route. Bentonite was selected as the support material because of its abundance, low cost, high surface area, and favorable adsorption properties.

Initially, 3 g of bentonite was dispersed in 50 mL of 0.05 M $SnCl_2 \cdot 5H_2O$ solution and vigorously stirred on a magnetic stirrer for 30 s at room temperature to obtain a homogeneous suspension, as shown in Figure 2c. Subsequently, 100 mL of *Murraya koenigii* leaf extract was added dropwise to the suspension over a period of 30 min under continuous stirring (Figure 2d). After 30 min, sodium hydroxide solution was gradually added until an alkaline pH was achieved. The reaction mixture was then continuously stirred for 5 h, during which light-colored precipitates were formed.

The resulting precipitates were separated by centrifugation at 4000 rpm for 20 min and filtered using Whatman filter paper. The filtrate obtained after the separation process is shown in Figure 2e. The collected precipitates were washed with distilled water and initially dried at room temperature, followed by drying at 80 °C in a vacuum oven for 48 h (Figure 2f). The dried material was subsequently calcined in a muffle furnace at 600 °C for 120 min. After calcination, the resulting material was ground to obtain a fine powdered SnO_2/bentonite nanocomposite (SBT-NC), as shown in Figure 2g.

The overall synthesis procedure and representative photographs of the *Murraya koenigii* extract, reaction mixture, filtration, drying, and final SBT-NC powder are presented in Figure 2.

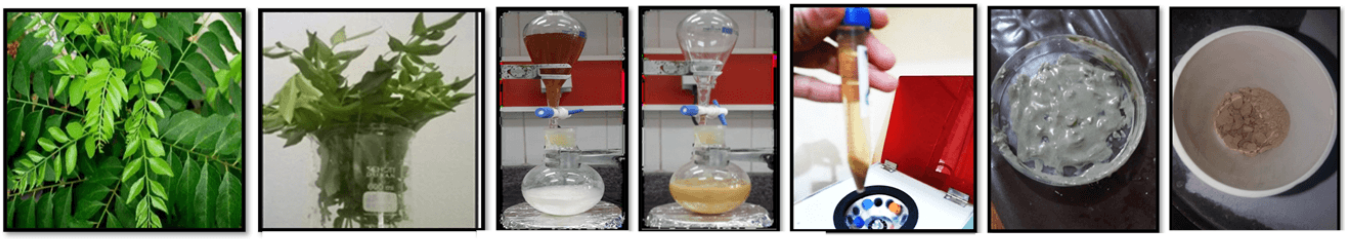

Figure 2 Stepwise procedure followed (a) curry leaves, (b)formation of extract, (c) Addition, (d) Mixing, (e) Centrifugation, (f) Filtration and (g) SBT-NC

3 Results and Discussion

3.1 Confirmation of synthesis

A green synthesis approach was employed for the preparation of SnO_2/bentonite nanocomposite using tin chloride pentahydrate, bentonite clay, and *Murraya koenigii* leaf extract. The prepared nanocomposite exhibited a high surface-to-volume ratio, which enhanced its adsorption capacity and sensitivity. Furthermore, the synthesized material demonstrated effective photocatalytic activity for wastewater treatment applications. The successful immobilization of SnO_2 nanoparticles onto the bentonite surface was confirmed through various characterization techniques.

The optical properties of the SnO_2/bentonite nanocomposite were investigated using UV–visible spectroscopy. The absorption spectra were recorded in the wavelength range of 200–800 nm. SnO_2 nanoparticles exhibited absorption mainly in the UV region due to their wide band gap, whereas the SBT-NC sample showed a broad absorption band extending into the visible region around 600 nm, which was attributed to surface plasmon resonance (SPR) effects. The maximum absorption peaks (λmax) were observed in the range of 270–530 nm. The UV absorption intensity was found to be dependent on the structural Sn(IV) concentration and inversely related to clay particle size.

The maximum absorption peak of the nanocomposite was observed at 337 nm (Figure 3), which was attributed to electron charge transfer processes involving transitions from the valence band to higher energy states. These electronic transitions resulted in the generation of photo-induced charge carriers, which subsequently reacted with oxygen and water molecules

at the surface to produce reactive oxygen species. These reactive radicals played a significant role in the degradation of pollutant molecules. The obtained results were consistent with previously reported studies, where SnO_2-related absorption peaks were observed around 350 nm, confirming the successful incorporation of SnO_2 nanoparticles within the bentonite matrix.

It was observed the absorption spectra of the SnO_2-bentonite composite shifting from 350 to 360 nm upon an increase in the SnO_2 content can be attributed to the band gap narrowing in relation to the interstitial SnO_2 species on the bentonite surface [57].

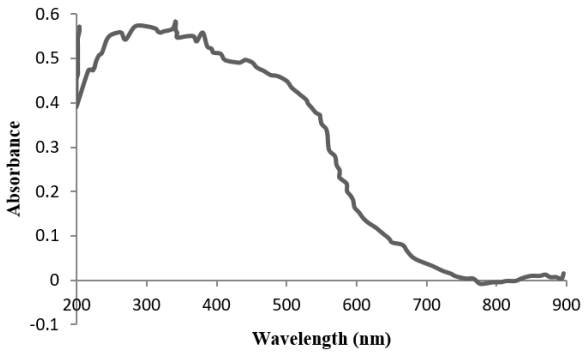

Figure 3 UV-Visible spectra of Tin oxide-bentonite composite

3.2 Scanning Electron Microscopy (SEM) analysis

SEM analysis was performed to investigate the morphological characteristics and particle size of the prepared materials. The SEM images of bentonite, SnO_2 nanoparticles, and SnO_2/bentonite nanocomposite are presented in Figure 4. The SEM micrographs revealed that natural bentonite consisted of layered nanoflakes of clay particles, indicating its porous structure and suitability as a support material for SnO_2 immobilization. The SnO_2 nanoparticles exhibited a predominantly spherical morphology with an average particle size of approximately 50 nm. Although the heterostructure of the composite was modified after incorporation of SnO_2 nanoparticles, the spherical SnO_2 particles were successfully distributed within the pores and surface of bentonite. The SEM images further showed that bentonite was a cohesive material composed of microsized agglomerates. The presence of interconnected pores in bentonite was also observed, which contributed to its enhanced adsorption capability toward various adsorbate molecules [58]. The SEM images of SnO_2-NP-AC at different resolutions from which a rough porous surface was observed which may be due to the loading of SnO_2 NPs on Activated Carbon surface [59]. It was also observed, spherical SnO_2 nanoparticles on bentonite in the SEM image of SnO2-bentonite nanocomposites [60].

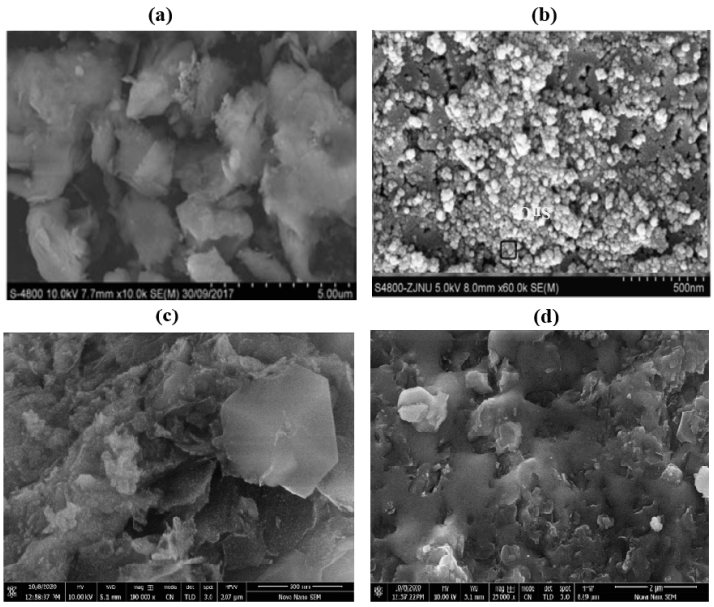

Figure 4 SEM Micrograph (a) Bentonite b) SnO_2, c) and d) SnO_2/bentonite nanocomposite (SBT-NC)

3.3 EDX analysis

Energy dispersive X-ray spectroscopy (EDX) analysis was performed to determine the elemental composition of the prepared SnO_2/bentonite nanocomposite, as presented in Figure 5. The EDX elemental mapping confirmed the presence of Fe, Ti, Ca, Mg, Na, O, C, Si, Al, and Sn within the nanocomposite. The EDX spectrum of SnO_2 nanoparticles showed characteristic peaks corresponding to tin (Sn) and oxygen (O), confirming the formation of SnO_2. In the case of bentonite, the detected elements mainly included Mg, O, Na, Al, and Si, which were associated with its clay composition. Furthermore, the appearance of Sn peaks in the SnO_2/bentonite nanocomposite, along with the characteristic elemental signals of bentonite, confirmed the successful incorporation and distribution of SnO_2 nanoparticles onto the bentonite matrix [61].

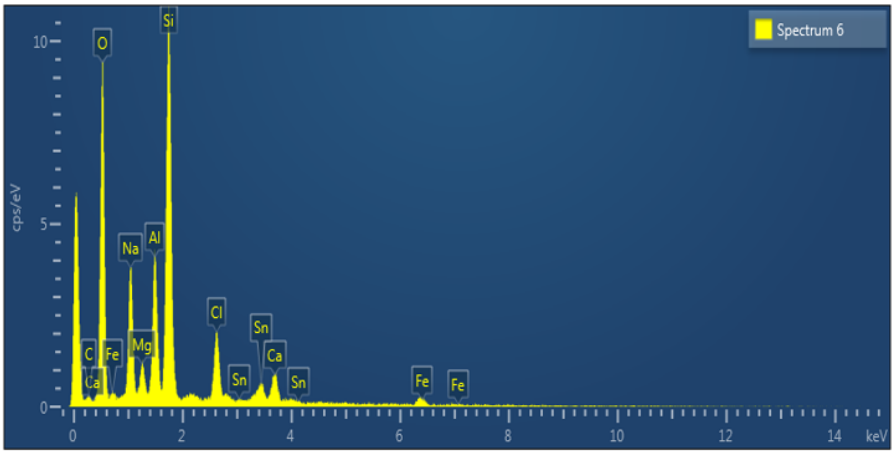

Figure 5 EDX Spectra of SnO_2/bentonite (SBT) nanocomposite

To analyze nanoparticles, composition at various calcination temperatures were analyzed by EDX spectroscopy that confirmed higher atomic content of oxygen than tin and peak at 0.3 keV respresented presence of carbon [62]. Bentonite was subjected to EDX analysis to determine the elemental composition. It was observed that untreated clay consisted of Na, Mg, Si, Al and all other elements. But after treatment, values of atomic content for Na and Mg has been decreased, confired the exchange of ions with protons [63].

3.4 FTIR analysis

The FTIR spectrum of bentonite is presented in Figure 6a, which revealed the characteristic functional groups and structural vibrations of the clay material. The broad absorption bands observed at 3452 and 1643 cm^{-1} were attributed to the stretching and bending vibrations of hydroxyl (–OH) groups, respectively, indicating the presence of adsorbed water molecules within the bentonite structure. The absorption bands located at 1030 and 1100 cm^{-1} were assigned to the stretching vibrations of Si–O–Si and Si–O bonds, while the band around 545 cm^{-1} corresponded to Si–O–Al bending vibrations.

The absorption peak observed at 3633 cm^{-1} was associated with the stretching vibration of hydroxyl groups bonded to Al^{3+} in the octahedral sheets of bentonite, whereas the band at 1644 cm^{-1} was related to the bending vibration of hydroxyl groups from interlayer water molecules. The bands at 3445 and 1428 cm^{-1} were attributed to O–H stretching vibrations of hydrated metal ions present in the bentonite layers and bending vibrations of water molecules associated with Al_2O_3 structures, respectively. The strong absorption band at 1048 cm^{-1} was assigned to the in-plane stretching vibration of Si–O bonds, while the peaks at 527 and 468 cm^{-1} were related to Si–O–Si and Al–O–Si vibrational modes, respectively. These characteristic bands confirmed the layered aluminosilicate structure of bentonite [64]. observed IR band at 1080 cm^{-1} that corresponds to Si-O-Si vibrations.

The FTIR spectrum for nanocomposite of SBT is shown in Figure 6b. In both of spectra, the absorption band at around 3654 cm^{-1} and 3437 cm^{-1} is related to free hydroxyl groups and the hydroxyl groups confirming the hydrogen bonding in these compounds, respectively. The typical band at 1654 cm^{-1} is corresponding to O-H bending vibrations of water. The absorption bands at around 1062, 534 and 487 cm^{-1} are due to Si–O–Si stretching vibrations and Si-O-Al and Si-O-Si bending vibrations, respectively. The band of Sn–O stretching vibrations should be

exhibited at around 511 cm^{-1}, but it overlaps with strong bands in this region and only causes the broadening of peaks.

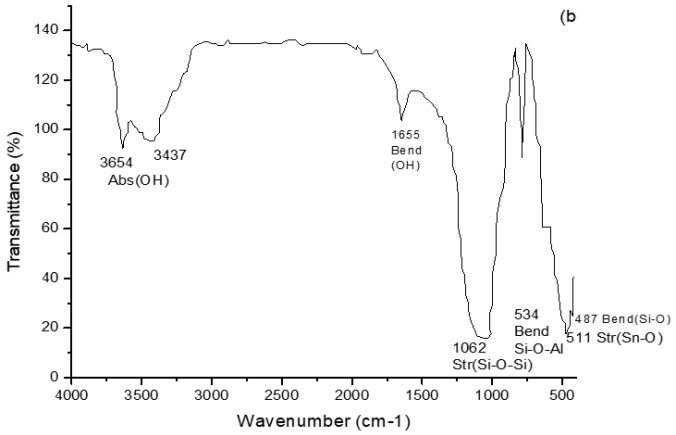

Figure 6 FT-IR spectra of a) Bentonite b) SBT-NCs

3.5 Optimization of the experimental variables

Various experimental variables like concentration, pH, dosage rate, effect of contact time on photocatalysis rate of Rhodamine B dye and Carbofuran pesticide. These parameters were optically optimized under study in following way:

3.5.1 Effect of pH

Strong effect of pH on the photodegradation efficiency of MB and Rh B solution was observed. The highest dye removal rate was obtained at pH of 10 and 11 for MB and Rh B respectively. For further increase in pH the degradation efficiency decreases. This observation indicates that efficient degradation of Rh B needs more basic solution as compared to MB. It is also observed that degradation is faster in alkaline medium as compared to acidic medium for both dyes. This phenomenon may be explained in terms of charge on ZrO_2. As ZrO_2 particles are either positively or negatively charged depending on the value of pH. As MB and Rh B are basic dyes and these produce cations in water so catalyst (ZrO_2 or ZrO_2/GR) repels MB and Rh B particles in acidic medium. Hence degradation was less in acidic medium [65].

Thus, at pH = 2.6, percentage removal of pesticide was high. The presence of greater positive charge sites on SBT surface, results in stronger electrostatic attraction among organic pollutants and positively charged SBT-NC. It was observed the effect of pH by changing the initial pH value of the pesticide solution from 2 to 5 and the results illustrated that degradation percentage of Carbofuran was increased at low pH range from 2-3 and it gave the highest degradation at pH 2.6. After increasing pH from 4 the degradation rate decreased. Therefore, the rate of CBF disappearance is strongly affected by the pH –dependence [66].

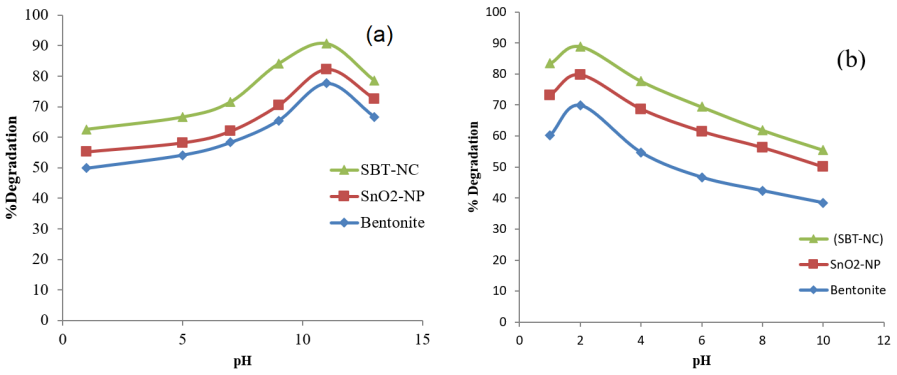

Figure 7 a) Effect of pH on the degradation of Rhodamine B dye; b) Effect of pH on the degradation of Carbofuran pesticide

Therefore, by keeping other variables constant, the optimum pH was evaluated. It is obvious that degradation of Rh B dye and CBF pesticide is affected by variation in pH. Results

showed bentonite and SnO_2-NPs didn't give high efficiency of degradation as compared to SnO_2/bentonite-NCs. The maximum degradation efficiency of Rhodamine B dye is in the following order 77.62 > 82.18 > and 90.71 for bentonite, SnO_2-NPs and SBT -NCs respectively as given in Figure 7a.

Figure 7b represented effect of pH on the degradation of CBF pesticide. The results revealed that at pH=2.6, the maximum degradation was observed. The maximum degradation efficiency is represented in the Figure 7b of Carbofuran in the following order 69.88 > 79.68 > and 90.13 for bentonite, SnO_2-NPs and SnO_2/bentonite -NCs respectively.

3.5.2 Effect of concentration

In present research, the initial concentration effect was seen through different treatment concentrations of Rhodamine B dye and Carbofuran pesticide (100, 80, 60, 40. 20 and 10 ppm) having photocatalysis at optimal time and pH under sunlight. it can be observed that maximum degradation is obtained at 10 ppm. As the dye concentration is increased keeping the catalyst amount constant, fewer active sites become available for the reaction. With increase in the number of dye molecules, the solution becomes more intensely colored and the path length of photons entering the solution decrease and fewer photons reach the catalyst surface, and the generation of hydroxyl and superoxide radicals gets reduced. Obtained results revealed that % degradation at 10 ppm concentration of Rh B dye was 60.08 > 71.76 and 86.37 for bentonite > SnO_2-NPs and SnO_2/bentonite -NCs respectively as shown in the Figure 8a.

It was observed the effect of initial Rh B concentration on the degradation by varying the concentration from 10 to 30 ppm, keeping the quantity of ZnO (200 mg/100 ml) constant. The degradation efficiency of Rh B was found to decrease with increase in the initial dye concentration . The active surface on the catalyst available for the reaction is critical for the degradation to take place . Incorporation of hydrogen peroxide within system favored the concentration increase of hydroxyl radicals which leads to quick pollutants decomposition. At still higher concentration of the dye, the (path length) surface area is further reduced and the Photodegradation was found to be negligible . The optimum concentration of dye was found to be 10 ppm [67].

While in the case of Carbofuran as shown in Figure 8b the maximum degradation is obtained at 10 ppm in the following order 51.33 <77.04 <87.14 for bentonite, SnO_2-NPs and SnO_2/bentonite -NCs respective1y for CBF pesticide. It was observed the effect of initial concentration of Carbofuran on the overall rate of degradation was studied by varying the initial concentration over a wide range from 10 to 100 mg l^{-1}. The results illustrated that rate of degradation decreases with increase in the carbofuran concentration up to 100 mg l^{-1}. The rate of degradation is related to the formation of OH radicals, which is the critical species in the degradation process. But above optimal concentration i.e 10 ppm the rate decreases due to insufficient quantity of OH radicals, as the formation of OH radicals is constant for a given amount of the catalyst [68].

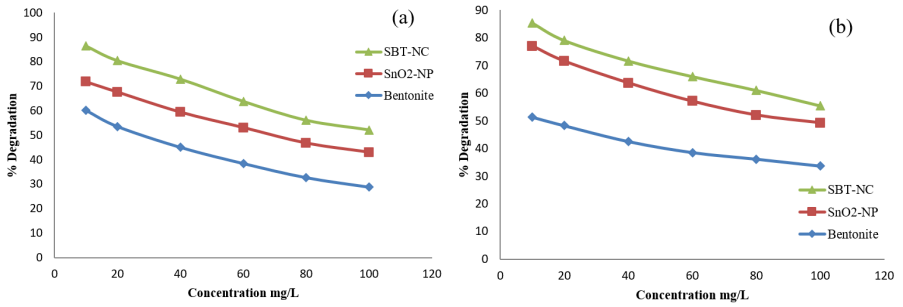

Figure 8 a) Effect of initial concentration for Rhodamine B dye degradation; b) Effect of initial concentration for the degradation of Carbofuran pesticide

3.5.3 Contact time

In current work, maximum efficiency for removal was obtained in 120 minutes. By keeping the experimental conditions constant, the contact time was studied. For instance, at pH of Rh B is 11, for CBF pesticide is at pH 2.6, concentration of dye and pesticide was 100ppm with dosage of 0.1g below sunlight. The uptake of dye/pesticide molecules on catalyst surface was due to more attractive forces that provides active sites for binding at initial contact time. However, with the passage of time, the availability of binding sites decreases and degradation

efficiency become constant after certain time.

The maximum % degradation is demonstrated in Figure 9a of Rhodamine B dye in the following order 69.11 < 83.63 < 92.15 for bentonite, SnO_2-NPs and SnO_2/bentonite-NCs respectively, where maximum removal was achieved at 90-120 min using SBT-NCs about 92.15% and at 90min confirmed that the SBT-NCs enhances the degradation efficiency during short time period. The maximum % degradation is showed in Figure 9b of Carbofuran pesticide in the following order 64.02 < 81.72 < 91.00 for bentonite, SnO_2-NPs and SnO_2/bentonite-NCs respectively.Results indicate highest degradation rate within 90 minutes by using photocatalysts.

It was observed the effects of contact time on the removal of Rh B using photocatalytic degradation by Na–Mt, BiOBr, and BiOBr–Mt. where all the degradation processes are rapid during the first 90 min period of reaction and the equilibrium is reached within 2 h. The fast degradation process at the initial stage (0–90 min) can be attributed to the fact that Rh B can interact easily with the reactive sites, while the slow degradation rate in later stage is mainly due to slower diffusion of solute into the interior of the photocatalysts [69].

It was observed the removal of carbofuran by activated carbon increased with time and then reached equilibrium at approximately 90 min. Furthermore, the removal was rapid in the early stages and reached an almost constant value over longer contact times. Obviously, the initial high degradation rate is due to the abundance of free binding sites [65]. The percentage degradation as evident from Figure 9 increases from 5 to 90 minutes and then after 120 minutes it remained unchanged. However, bentonite based SnO_2 nanocomposites, degradation efficiency was obtained 92.15% for Rhodamine B dye and 91.01% for Carbofuran pesticide which indicated that SnO_2/bentonite-NCs enhanced the degradation under sunlight effectively.

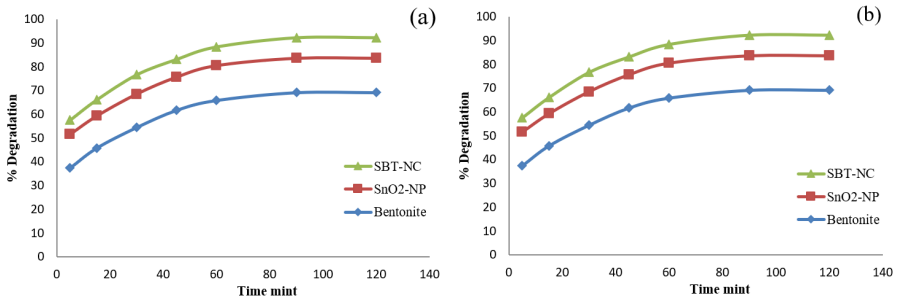

Figure 9 a) Relation between contact time and Rhodamine B dye degradation; b) Effect of contact time on degradation of Carbofuran pesticide

3.5.4 Effect of dose rate

The effect of catalyst dosage on the photocatalytic degradation of Carbofuran was investigated. Catalyst loading is an important parameter that influences degradation efficiency; however, excessive catalyst concentration can reduce cost-effectiveness and increase solution turbidity. An increase in catalyst dosage initially enhanced the degradation rate due to the availability of more active sites and increased generation of reactive species on the photocatalyst surface. The optimum catalyst dosage was found to be 0.1 g/L, which provided maximum degradation efficiency.

The improved photocatalytic performance at higher catalyst loading was attributed to the increased number of irradiated active sites and the greater availability of reactive species relative to pollutant molecules. However, further increase in catalyst concentration resulted in a decline in degradation efficiency. This reduction was associated with particle agglomeration caused by attractive forces between catalyst particles, which decreased the available active surface area. Moreover, excessive catalyst loading increased the turbidity of the reaction mixture, limiting light penetration and reducing photon absorption by the catalyst surface [70]. Optimum dose rate was found to be 0.1 g-0.2 g. The catalyst amount inside mixture converts into active site available for the process of degradation, thus, uptake of pollutant increases with dosage increase as shown in figure. The dose increased to 0.2g from 0.05 g at 3 or 4 pH. Thus, 0.1-0.2 g of dose rate was chosen as catalyst dose for all experiments with fixed dose amount due to higher percentage degradation [71].

In Figure 10, by increasing dose rate of catalysts, the %degradation efficiency was increased and then decreased. At 0.1g, the %degradation for bentonite was 71.14%, for SnO_2-NPs 84.03% and by using SnO_2/bentonite-NCs %degradation was increased upto maximum value of 93.12%

of rhodamine b dye. At 0.1g, the %degradation for bentonite was 70.86%, for SnO_2-NPs 82.50% and by using SnO_2/bentonite-NCs %degradation was increased up to 90.42% maximum value of carbofuran pesticide. The obtained results showed that %degradation of Rh B and CBF pesticide was 71.14 > 84.02 > 93.12 and 70.86 > 82.50 > 90.42 for bentonite> SnO_2-NPs and SnO_2/bentonite-NCs respective1y. From the results, it is clear that by increasing dose rate the degradation efficiency was decrease because the surface area on the surface of catalyst increased but at the same time turbidity of suspension also increased. Therefore, penetration power of ultraviolet light decreased due to increase the tyndall effect.

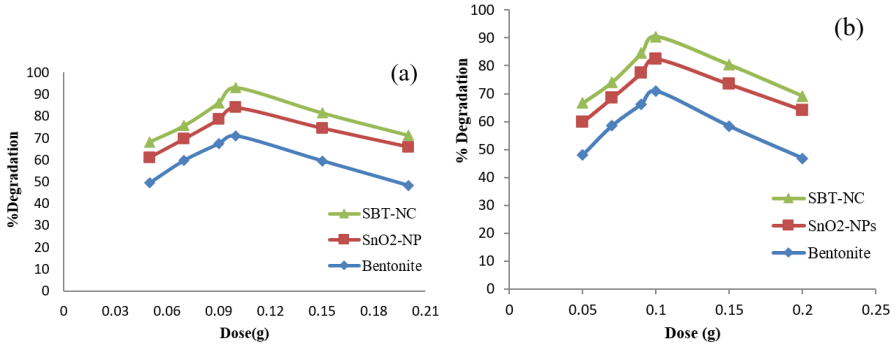

Figure 10 a) Effect of dose rate on degradation of Rhodamine B dye degradation; b) Effect of dose rate on degradation of Carbofuran pesticide

3.6 Comparison among different catalysts

A comparative study was performed to evaluate the photocatalytic degradation efficiency of bentonite, SnO_2 nanoparticles, and SnO_2/bentonite nanocomposite (SBT-NC) toward Rhodamine B dye and Carbofuran pesticide. The degradation performance of different catalysts is compared in Figure 11. The results demonstrated that SBT-NC exhibited significantly higher photocatalytic activity compared with individual bentonite and SnO_2 nanoparticles. Under optimized conditions of pH, pollutant concentration, contact time, and catalyst dosage, the maximum degradation efficiencies achieved by SBT-NC were 92.87% for Rhodamine B dye and 90.50% for Carbofuran pesticide. In comparison, bentonite showed degradation efficiencies of 68.81% and 65.02% for Rhodamine B and Carbofuran, respectively, whereas SnO_2 nanoparticles exhibited 84.60% and 80.89% degradation efficiency for the respective pollutants.

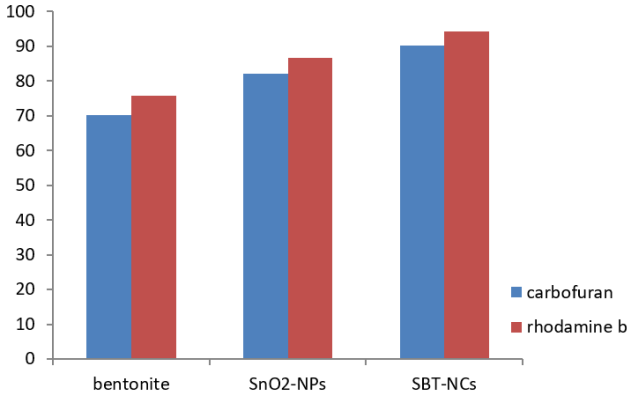

Figure 11 Effect of different catalysts on degradation of Rhodamine B dye and Carbofuran pesticide

The enhanced photocatalytic performance of SBT-NC was attributed to the synergistic interaction between SnO_2 nanoparticles and bentonite, which improved pollutant adsorption, increased available active sites, and facilitated photocatalytic reactions. Compared with previously reported clay-supported metal oxide photocatalysts, the prepared SnO_2/bentonite nanocomposite demonstrated rapid degradation of both dye and pesticide pollutants. Furthermore, while SnO_2 nanoparticles generally require UV irradiation for photocatalytic activation, the SBT-NC exhibited improved light utilization and enhanced degradation efficiency under visible light irradiation, indicating its potential for efficient wastewater treatment applications.

3.7 Kinetic study of degradation of Rhodamine B and Carbofuran by SBT NC

The kinetic parameters for the photocatalytic degradation of Rhodamine B dye and Carbofuran pesticide using the synthesized nanocomposite were evaluated under different experimental conditions using response surface methodology. The degradation kinetics were analyzed using pseudo-first-order, pseudo-second-order, and Bangham kinetic models. For the first-order kinetic model, the relationship between $\ln(C_0/Ct)$ and reaction time (t) was evaluated, while the second-order kinetic model was studied by plotting t versus $[(1/Ct)-(1/C_0)]$. The Bangham model was analyzed using the relationship between t and $t/[1-(Ct-C_0)]$.

The validity and suitability of each kinetic model were determined based on the regression correlation coefficient (R^2) values obtained from the kinetic plots. The results revealed that the R^2 values for the first-order kinetic model were greater than 0.98, which were higher than those obtained for the second-order and Bangham models. This indicated that the photocatalytic degradation of Rhodamine B and Carbofuran followed first-order reaction kinetics.

The calculated kinetic parameters, including rate constants and correlation coefficients, are presented in Table 2. The lower R^2 values obtained for the second-order and Bangham kinetic models indicated poor agreement between the experimental data and these models. In contrast, the first-order kinetic model showed the best fitting with the experimental degradation data. Therefore, the photocatalytic degradation process of Rhodamine B dye and Carbofuran pesticide over the SnO_2/bentonite nanocomposite was better described by the first-order kinetic model. (see Figure 12, 13, and 14)

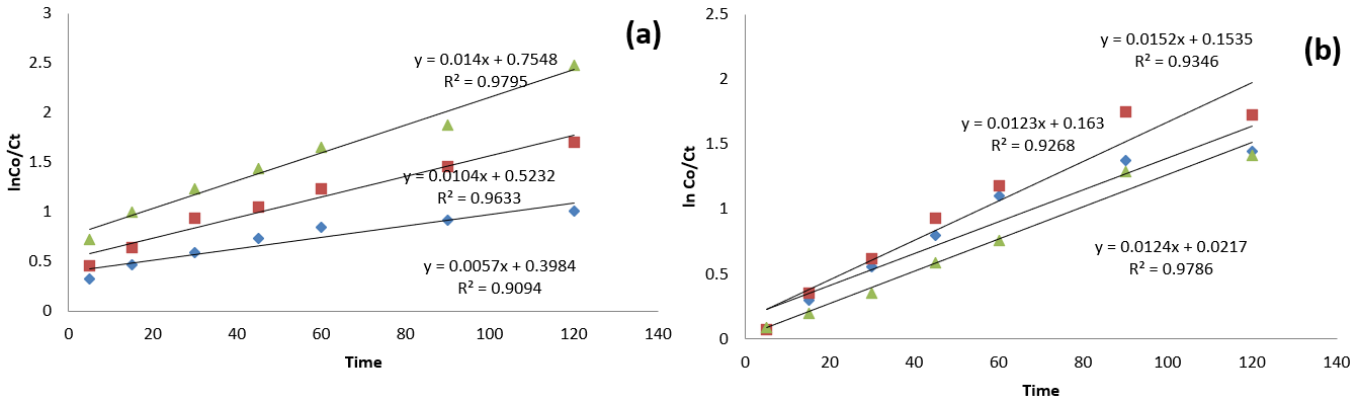

Figure 12 Pseudo 1^{st} order kinetics of (a) Rhodamine B dye and (b) Carbofuran pesticide

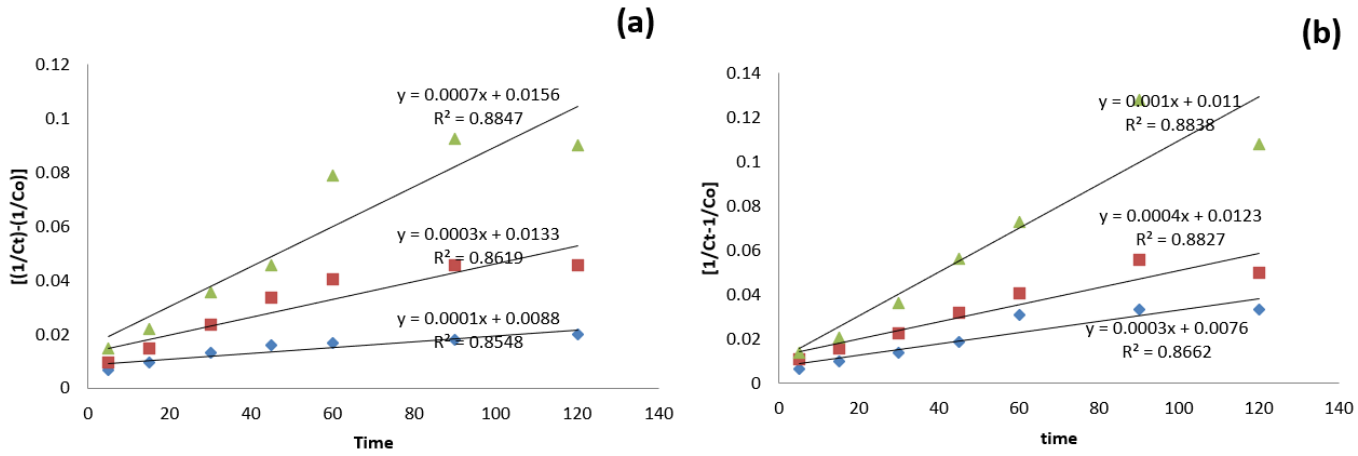

Figure 13 Pseudo 2^{nd} order kinetics of (a) Rhodamine B dye (b) Carbofuran pesticide

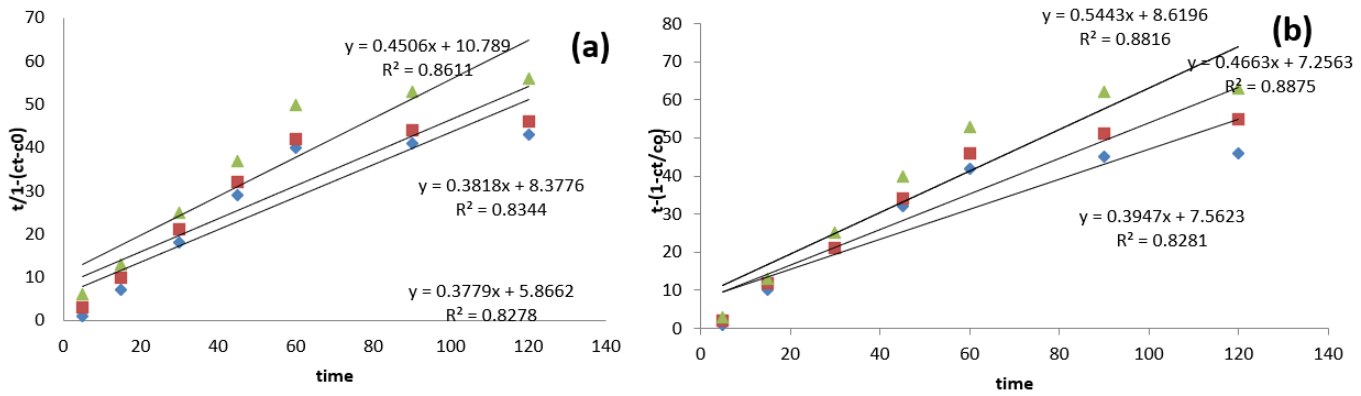

Figure 14 Pseudo 2^{nd} order kinetics of (a) Rhodamine B dye (b) Carbofuran pesticide

Table 2 Kinetic models for degradation of Rhodamine B dye and Carbofuran pesticide

Dyes	Catalysts	First Order Kinetic Model		Second Order Kinetic Model		BMG Kinetic Model		
		K_1/min^{-1}	R^2	$K_2/M^{-1}min^{-1}$	R^2	1/m	1/b	R^2
Carbofuran pesticide	Bentonite	0.0053409	0.9268	0.000012	0.8662	0.13223	2.53356	0.8281
	SnO_2-NPs	0.0066001	0.9346	0.000013	0.8827	0.13781	2.1445	0.8875
	SnO_2/bentonite –NCs	0.005384281	0.9786	0.0000675	0.8838	0.11601	1.80407	0.8816
Rhodamine B dye	Bentonite	0.002475033	0.9094	0.00008155	0.8548	0.17046	2.64620	0.8278
	SnO_2-NPs	0.004515849	0.9633	0.000206728	0.8619	0.119365	2.619170	0.8344
	SnO_2/bentonite –NCs	0.006079027	0.9795	0.000259671	0.9947	0.09268	2.2192	0.8611

4 Conclusion

Water pollution resulting from synthetic dyes and agricultural pesticides represents a significant environmental challenge because of the toxic and persistent nature of these contaminants. In the present study, SnO_2 nanoparticles and a SnO_2/bentonite nanocomposite (SBT-NC) were successfully synthesized using a green approach involving *Murraya koenigii* leaf extract. The prepared materials were characterized using UV–visible spectroscopy, SEM, EDX, and FTIR, and the results confirmed the formation of SnO_2 nanoparticles and their successful incorporation onto the bentonite support. The photocatalytic degradation experiments demonstrated that the SnO_2/bentonite nanocomposite exhibited superior performance compared with pure bentonite and SnO_2 nanoparticles for both Rhodamine B dye and Carbofuran pesticide. The degradation efficiency was strongly influenced by pH, initial pollutant concentration, contact time, and catalyst dosage. The optimum catalyst dosage was approximately 0.1 g, while maximum degradation occurred within approximately 90–120 min. Rhodamine B showed the highest degradation under alkaline conditions at approximately pH 11, whereas Carbofuran showed maximum degradation under acidic conditions at approximately pH 2.6.

Under the optimized experimental conditions, SBT-NC achieved approximately 92–94% degradation of Rhodamine B and approximately 90–91% degradation of Carbofuran, demonstrating its superior photocatalytic activity. The enhanced performance of the nanocomposite can be attributed to the synergistic contribution of SnO_2 and bentonite. Bentonite provided adsorption sites and a suitable support for the dispersion of SnO_2 nanoparticles, while SnO_2 promoted photocatalytic reactions through the generation of photo-induced electron–hole pairs and reactive oxygen species. The kinetic investigation further indicated that the degradation behavior was generally better represented by the pseudo-first-order kinetic model. Overall, the findings demonstrate that green-synthesized SnO_2/bentonite nanocomposite is a promising, sustainable, and effective material for the treatment of wastewater contaminated with organic pollutants. The use of *Murraya koenigii* leaf extract provides an environmentally friendly synthesis route, while the combination of SnO_2 and naturally abundant bentonite enhances pollutant removal. Therefore, SBT-NC has considerable potential for application in wastewater remediation and environmental protection.

Conflicts of Interest

The authors declare that they have no conflicts of interest.

References

[1] Elumalai P, Gao X, Parthipan P, et al. Agrochemical pollution: A serious threat to environmental health. Current Opinion in Environmental Science & Health. 2025, 43: 100597. https://doi.org/10.1016/j.coesh.2025.100597

[2] Zulfiqar N. Synthesis and Characterization of Pure and Zirconium Doped NiO-ZnO Nanocomposite for the Photodegradation of Brilliant Green Dye. Published online 2023. https://doi.org/10.2139/ssrn.4582129

[3] Zulfiqar N. Industrial and Agricultural Contributions to Water Pollution in Pakistan: Policy Interventions for Sustainable Water Management , Published online 2025. https://doi.org/10.2139/ssrn.5294649

[4] Abdel-Messih MF, Ahmed MA, El-Sayed AS. Photocatalytic decolorization of Rhodamine B dye using novel mesoporous SnO2–TiO2 nano mixed oxides prepared by sol–gel method. Journal of Photochemistry and Photobiology A: Chemistry. 2013, 260: 1-8. https://doi.org/10.1016/j.jphotochem.2013.03.011

[5] Saini J, Garg VK, Gupta RK, et al. Removal of Orange G and Rhodamine B dyes from aqueous system using hydrothermally synthesized zinc oxide loaded activated carbon (ZnO-AC). Journal of Environmental Chemical Engineering. 2017, 5(1): 884-892. https://doi.org/10.1016/j.jece.2017.01.012

[6] Xu X, Liu Y, Liu S, et al. Real-time detection of potable-reclaimed water pipe cross-connection events by conventional water quality sensors using machine learning methods. Journal of Environmental Management. 2019, 238: 201-209. https://doi.org/10.1016/j.jenvman.2019.02.110

[7] Amoli-Diva M, Anvari A, Sadighi-Bonabi R. Synthesis of magneto-plasmonic Au-Ag NPs-decorated TiO2-modified Fe3O4 nanocomposite with enhanced laser/solar-driven photocatalytic activity for degradation of dye pollutant in textile wastewater. Ceramics International. 2019, 45(14): 17837-17846. https://doi.org/10.1016/j.ceramint.2019.05.355

[8] Pathania D, Gupta D, Al-Muhtaseb AH, et al. Photocatalytic degradation of highly toxic dyes using chitosan-g-poly(acrylamide)/ZnS in presence of solar irradiation. Journal of Photochemistry and Photobiology A: Chemistry. 2016, 329: 61-68. https://doi.org/10.1016/j.jphotochem.2016.06.019

[9] Peng L, Zheng R-r, Feng D-w, et al. Synthesis of eco-friendly porous g-C3N4/SiO2/SnO2 composite with excellent visible-light responsive photocatalysis. Arabian Journal of Chemistry. 2020, 13(2): 4275-4285. https://doi.org/10.1016/j.arabjc.2019.07.009

[10] Singh J, Kaur N, Kaur P, et al. Piper betle leaves mediated synthesis of biogenic SnO2 nanoparticles for photocatalytic degradation of reactive yellow 186 dye under direct sunlight. Environmental Nanotechnology, Monitoring & Management. 2018, 10: 331-338. https://doi.org/10.1016/j.enmm.2018.07.001

[11] Sobhani-Nasab A, Behvandi S, Karimi MA, et al. Synergetic effect of graphene oxide and C3N4 as co-catalyst for enhanced photocatalytic performance of dyes on Yb2(MoO4)3/YbMoO4 nanocomposite. Ceramics International. 2019, 45(14): 17847-17858. https://doi.org/10.1016/j.ceramint.2019.05.356

[12] Thakur M, Sharma G, Ahamad T, et al. Efficient photocatalytic degradation of toxic dyes from aqueous environment using gelatin-Zr(IV) phosphate nanocomposite and its antimicrobial activity. Colloids and Surfaces B: Biointerfaces. 2017, 157: 456-463. https://doi.org/10.1016/j.colsurfb.2017.06.018

[13] Thangavel S, Venugopal G, Kim S-J. Enhanced photocatalytic efficacy of organic dyes using β-tin tungstate–reduced graphene oxide nanocomposites. Materials Chemistry and Physics. 2014, 145(1-2): 108-115. https://doi.org/10.1016/j.matchemphys.2014.01.046

[14] Wang Y, Yang Q, Wang X, et al. Photocatalytic degradation of rhodamin B and diclofenac sodium on hollow hierarchical microspheres of BiOBr modified with sepiolite and polyvinyl pyrrolidone (PVP). Materials Science and Engineering: B. 2019, 244: 12-22. https://doi.org/10.1016/j.mseb.2019.04.005

[15] Huang H, Zhang J, Jiang L, et al. Preparation of cubic Cu2O nanoparticles wrapped by reduced graphene oxide for the efficient removal of rhodamine B. Journal of Alloys and Compounds. 2017, 718: 112-115. https://doi.org/10.1016/j.jallcom.2017.05.132

[16] Tuzen M, Sarı A, Saleh TA. Response surface optimization, kinetic and thermodynamic studies for effective removal of rhodamine B by magnetic AC/CeO2 nanocomposite. Journal of Environmental Management. 2018, 206: 170-177. https://doi.org/10.1016/j.jenvman.2017.10.016

[17] Hassanpour M, Safardoust-Hojaghan H, Salavati-Niasari M. Degradation of methylene blue and Rhodamine B as water pollutants via green synthesized Co3O4/ZnO nanocomposite. Journal of Molecular Liquids. 2017, 229: 293-299. https://doi.org/10.1016/j.molliq.2016.12.090

[18] Singh BR, Shoeb Mohd, Khan W, et al. Synthesis of graphene/zirconium oxide nanocomposite photocatalyst for the removal of rhodamineB dye from aqueous environment. Journal of Alloys and Compounds. 2015, 651: 598-607.
https://doi.org/10.1016/j.jallcom.2015.05.231

[19] Chook SW, Chia CH, Chan CH, et al. A porous aerogel nanocomposite of silver nanoparticles-functionalized cellulose nanofibrils for SERS detection and catalytic degradation of rhodamine B. RSC Advances. 2015, 5(108): 88915-88920.
https://doi.org/10.1039/c5ra18806g

[20] Oyetade OA, Nyamori VO, Martincigh BS, et al. Effectiveness of carbon nanotube–cobalt ferrite nanocomposites for the adsorption of rhodamine B from aqueous solutions. RSC Advances. 2015, 5(29): 22724-22739.
https://doi.org/10.1039/c4ra15446k

[21] Rani S, Aggarwal M, Kumar M, et al. Removal of methylene blue and rhodamine B from water by zirconium oxide/graphene. Water Science. 2016, 30(1): 51-60.
https://doi.org/10.1016/j.wsj.2016.04.001

[22] Khan UA, Liu J, Pan J, et al. Fabrication of floating CdS/EP photocatalyst by facile liquid phase deposition for highly efficient degradation of Rhodamine B (RhB) under visible light irradiation. Materials Science in Semiconductor Processing. 2018, 83: 201-210.
https://doi.org/10.1016/j.mssp.2018.04.028

[23] Sundararajan M, Kennedy LJ. Photocatalytic removal of rhodamine B under irradiation of visible light using Co1Cu Fe2O4 ($0 \leq x \leq 0.5$) nanoparticles. Journal of Environmental Chemical Engineering. 2017, 5(4): 4075-4092.
https://doi.org/10.1016/j.jece.2017.07.054

[24] Sharma G, Dionysiou DD, Sharma S, et al. Highly efficient Sr/Ce/activated carbon bimetallic nanocomposite for photoinduced degradation of rhodamine B. Catalysis Today. 2019, 335: 437-451.
https://doi.org/10.1016/j.cattod.2019.03.063

[25] Mohamed Jaffer Sadiq M, Samson Nesaraj A. Soft chemical synthesis and characterization of BaWO4 nanoparticles for photocatalytic removal of Rhodamine B present in water sample. Journal of Nanostructure in Chemistry. 2014, 5(1): 45-54.
https://doi.org/10.1007/s40097-014-0133-y

[26] Belachew N, Rama Devi D, Basavaiah K. Green synthesis and characterisation of L-Serine capped magnetite nanoparticles for removal of Rhodamine B from contaminated water. Journal of Experimental Nanoscience. 2017, 12(1): 114-128.
https://doi.org/10.1080/17458080.2017.1279354

[27] Ji K, Deng J, Zang H, et al. Fabrication and high photocatalytic performance of noble metal nanoparticles supported on 3DOM InVO4–BiVO4 for the visible-light-driven degradation of rhodamine B and methylene blue. Applied Catalysis B: Environmental. 2015, 165: 285-295.
https://doi.org/10.1016/j.apcatb.2014.10.005

[28] Yao S, Xu L, Gao Q, et al. Enhanced photocatalytic degradation of Rhodamine B by reduced graphene oxides wrapped-Cu2SnS3 flower-like architectures. Journal of Alloys and Compounds. 2017, 704: 469-477.
https://doi.org/10.1016/j.jallcom.2017.02.069

[29] Xu W, Fang J, Chen Y, et al. Novel heterostructured Bi2S3/Bi2Sn2O7 with highly visible light photocatalytic activity for the removal of rhodamine B. Materials Chemistry and Physics. 2015, 154: 30-37.
https://doi.org/10.1016/j.matchemphys.2015.01.040

[30] Wu Z, Yuan X, Zhong H, et al. Effective removal of high-chroma rhodamine B over Sn 0.215 In 0.38 S/reduced graphene oxide composite: Synergistic factors and mechanism of adsorption enrichment and visible photocatalytic degradation. Powder Technology. 2018, 329: 217-231.
https://doi.org/10.1016/j.powtec.2018.01.046

[31] Wang S, Yang B, Liu Y. Synthesis of a hierarchical SnS2 nanostructure for efficient adsorption of Rhodamine B dye. Journal of Colloid and Interface Science. 2017, 507: 225-233.
https://doi.org/10.1016/j.jcis.2017.07.053

[32] Manukumar KN, Nagaraju G, Kishore B, et al. Ionic liquid-assisted hydrothermal synthesis of SnS nanoparticles: Electrode materials for lithium batteries, photoluminescence and photocatalytic activities. Journal of Energy Chemistry. 2018, 27(3): 806-812.
https://doi.org/10.1016/j.jechem.2017.05.010

[33] Song Y, Gu J, Xia K, et al. Construction of 2D SnS2/g-C3N4 Z-scheme composite with superior visible-light photocatalytic performance. Applied Surface Science. 2019, 467-468: 56-64.
https://doi.org/10.1016/j.apsusc.2018.10.118

[34] Khandekar DC, Bhattacharyya AR, Bandyopadhyaya R. Role of impregnated nano-photocatalyst (SnxTi(1-x)O2) inside mesoporous silica (SBA-15) for degradation of organic pollutant (Rhodamine B) under UV light. Journal of Environmental Chemical Engineering. 2019, 7(5): 103433.
https://doi.org/10.1016/j.jece.2019.103433

[35] Zulfiqar N, Ali M, Inam F, et al. Synthesis of metal nanoparticles and their role in degradation of pesticides/herbicides: a review. Discover Applied Sciences. 2025, 7(6).
https://doi.org/10.1007/s42452-025-07089-9

[36] Djellabi R, Ghorab MF, Cerrato G, et al. Photoactive TiO2–montmorillonite composite for degradation of organic dyes in water. Journal of Photochemistry and Photobiology A: Chemistry. 2014, 295: 57-63.
https://doi.org/10.1016/j.jphotochem.2014.08.017

[37] Zulfiqar N, Asad Ali M, Rafique F, et al. Sustainable Fabrication of Metal-doped rGO Nanocomposites for Photocatalytic Antibiotic Degradation in Aqueous Systems. Advance in Sustainability. 2025, 5(1): 18-27.
https://doi.org/10.26855/as.2025.06.003

[38] Zulfiqar N, Inam F, Khudayberganov I, et al. Sustainable synthesis and photocatalytic insights into Ag-doped copper oxide nanoparticles: a comparative study. Scientific Reports. 2026, 16(1).
https://doi.org/10.1038/s41598-025-32715-2

[39] Zulfiqar N, Nadeem R, Musaimi OA. Photocatalytic Degradation of Antibiotics via Exploitation of a Magnetic Nanocomposite: A Green Nanotechnology Approach toward Drug-Contaminated Wastewater Reclamation. ACS Omega. Published online February 6, 2024.
https://doi.org/10.1021/acsomega.3c08116

[40] Zulfiqar N, Shariatipour M, Inam F. Sequestration of chromium(vi) and nickel(ii) heavy metals from unhygienic water via sustainable and innovative magnetic nanotechnology. Nanoscale Advances. 2024, 6(1): 287-301.
https://doi.org/10.1039/d3na00923h

[41] Santhosh C, Velmurugan V, Jacob G, et al. Role of nanomaterials in water treatment applications: A review. Chemical Engineering Journal. 2016, 306: 1116-1137.
https://doi.org/10.1016/j.cej.2016.08.053

[42] Duran C, Ozdes D, Bulut VN, et al. Cloud-point extraction of rhodamine 6G by using Triton X-100 as the non-ionic surfactant. Journal of AOAC International, 2011, 94(1): 286-292.
https://doi.org/10.1093/jaoac/94.1.286

[43] Yu J-X, He Z-Y, Qi Y-F, et al. Regeneration of Rhodamine B Loaded Modified Biosorbent by a Self-Cleaning Eluent: TiO2 Hydrosol. CLEAN - Soil, Air, Water. 2011, 39(4): 400-405.
https://doi.org/10.1002/clen.201000045

[44] Chen X, Zhou Q, Liu F, et al. Removal of nine pesticide residues from water and soil by biosorption coupled with degradation on biosorbent immobilized laccase. Chemosphere. 2019, 233: 49-56.
https://doi.org/10.1016/j.chemosphere.2019.05.144

[45] Ahmed Ibrahim KE, Şolpan D. Removal of carbofuran in aqueous solution by using UV-irradiation/hydrogen peroxide. Journal of Environmental Chemical Engineering. 2019, 7(1): 102820.
https://doi.org/10.1016/j.jece.2018.102820

[46] Chen J-q, Hu Z-j, Ji R. Removal of carbofuran from aqueous solution by orange peel. Desalination and Water Treatment. 2012, 49(1-3): 106-114.
https://doi.org/10.1080/19443994.2012.708205

[47] Singh RK, Philip L, Ramanujam S. Rapid Removal of Carbofuran from Aqueous Solution by Pulsed Corona Discharge Treatment: Kinetic Study, Oxidative, Reductive Degradation Pathway, and Toxicity Assay. Industrial & Engineering Chemistry Research. 2016, 55(26): 7201-7209.
https://doi.org/10.1021/acs.iecr.6b01191

[48] Roudani A, Mamouni R, Saffaj N, et al. Removal of Carbofuran Pesticide from Aqueous Solution by Adsorption onto Animal Bone Meal as New Low Cost Adsorbent. Chemical and Process Engineering Research. 2014, 28(2014): 32-44.
https://iiste.org/Journals/index.php/CPER/article/view/17091/1

[49] Arya S, Lehana PK, Rana SB. Synthesis of Zinc Oxide Nanoparticles and Their Morphological, Optical, and Electrical Characterizations. Journal of Electronic Materials. 2017, 46(7): 4604-4611.
https://doi.org/10.1007/s11664-017-5469-x

[50] Yang L, Chen S, Hu M, et al. Biodegradation of carbofuran by Pichia anomala strain HQ-C-01 and its application for bioremediation of contaminated soils. Biology and Fertility of Soils. 2011, 47(8): 917-923.
https://doi.org/10.1007/s00374-011-0602-0

[51] Kanan S, Moyet MA, Arthur RB, et al. Recent advances on TiO 2 -based photocatalysts toward the degradation of pesticides and major organic pollutants from water bodies. Catalysis Reviews. 2019, 62(1): 1-65.
https://doi.org/10.1080/01614940.2019.1613323

[52] Keçili R, Büyüktiryaki S, Hussain CM. Advancement in bioanalytical science through nanotechnology: Past, present and future. TrAC Trends in Analytical Chemistry. 2019, 110: 259-276.
https://doi.org/10.1016/j.trac.2018.11.012

[53] Nasrollahzadeh M, Issaabadi Z, Sajjadi M, et al. Types of Nanostructures. An Introduction to Green Nanotechnology. Published online 2019: 29-80.
https://doi.org/10.1016/b978-0-12-813586-0.00002-x

[54] Ullah Z. Nanotechnology and its impact on modern computer. Global Journal of Research In Engineering. 2013, 12(4-J).
https://globaljournals.org

[55] Abdennouri M, Baâlala M, Galadi A, et al. Photocatalytic degradation of pesticides by titanium dioxide and titanium pillared purified clays. Arabian Journal of Chemistry. 2016, 9: S313-S318.
https://doi.org/10.1016/j.arabjc.2011.04.005

[56] Bai S, Chu H, Xiang X, et al. Fabricating of Fe2O3/BiVO4 heterojunction based photoanode modified with NiFe-LDH nanosheets for efficient solar water splitting. Chemical Engineering Journal. 2018, 350: 148-156.
https://doi.org/10.1016/j.cej.2018.05.109

[57] Bajaj G, Soni RK. Synthesis of composite gold/tin-oxide nanoparticles by nano-soldering. Journal of Nanoparticle Research. 2010, 12(7): 2597-2603.
https://doi.org/10.1007/s11051-009-9836-2

[58] Tran TTT, Doan VD, Ho TTT, et al. Novel of TiO 2 /Ag 3 PO 4 /Bentonite Composite Photocatalyst: Preparation, Characterization, and Application for Degradation of Methylene Blue in Aqueous Solution. Environmental Engineering Science. 2019, 36(1): 71-80.
https://doi.org/10.1089/ees.2018.0179

[59] Begum S, Ahmaruzzaman Md. Green Synthesis of SnO 2 Nanoparticles loaded on Activated Carbon and its Application as Photocalayst in the Degradation of Alizarin Red S Dye. Materials Today: Proceedings. 2018, 5(1): 2314-2320.
https://doi.org/10.1016/j.matpr.2017.09.235

[60] Hristodor CM, Vrinceanu N, Copcia VE, et al. Photocatalytic degradation of Eosin Y dye using SnO 2 nanocomposites.
https://www.romnet.net

[61] Absalan S, Nasresfahani Sh, Sheikhi MH. High-performance carbon monoxide gas sensor based on palladium/tin oxide/porous graphitic carbon nitride nanocomposite. Journal of Alloys and Compounds. 2019, 795: 79-90.
https://doi.org/10.1016/j.jallcom.2019.04.187

[62] Cruz A, Couto L, Esplugas S, et al. Study of the contribution of homogeneous catalysis on heterogeneous Fe(III)/alginate mediated photo-Fenton process. Chemical Engineering Journal. 2017, 318: 272-280.
https://doi.org/10.1016/j.cej.2016.09.014

[63] Das PS, Bakuli S, Biswas I, et al. RGO/MgO hybrid nanocomposites with high specific capacitance. Ceramics International. 2018, 44(1): 424-432.
https://doi.org/10.1016/j.ceramint.2017.09.194

[64] Martínez-Costa JI, Rivera-Utrilla J, Leyva-Ramos R, et al. Individual and simultaneous degradation of antibiotics sulfamethoxazole and trimethoprim by UV and solar radiation in aqueous solution using bentonite and vermiculite as photocatalysts. Applied Clay Science. 2018, 160: 217-225.
https://doi.org/10.1016/j.clay.2017.12.026

[65] Rani M, Rachna, Shanker U. Metal oxide-chitosan based nanocomposites for efficient degradation of carcinogenic PAHs. Journal of Environmental Chemical Engineering. 2020, 8(3): 103810.
https://doi.org/10.1016/j.jece.2020.103810

[66] Ferdoush F, Katsumata H, Russel M, et al. Degradation of carbofuran by V(IV)/H2O2 system in aqueous solution. Bangladesh Journal of Scientific and Industrial Research. 2015, 50(3): 211-218.
https://doi.org/10.3329/bjsir.v50i3.25588

[67] Danwittayakul S, Jaisai M, Dutta J. Efficient solar photocatalytic degradation of textile wastewater using ZnO/ZTO composites. Applied Catalysis B: Environmental. 2015, 163: 1-8.
https://doi.org/10.1016/j.apcatb.2014.07.042

[68] Khan H, Khalil AK, Khan A. Photocatalytic degradation of alizarin yellow in aqueous medium and real samples using chitosan conjugated tin magnetic nanocomposites. Journal of Materials Science: Materials in Electronics. 2019, 30(24): 21332-21342.
https://doi.org/10.1007/s10854-019-02510-7

[69] Chu J, Wang X, Wang D, et al. Highly selective detection of sulfur hexafluoride decomposition components H2S and SOF2 employing sensors based on tin oxide modified reduced graphene oxide. Carbon. 2018, 135: 95-103.
https://doi.org/10.1016/j.carbon.2018.04.037

[70] Haritha E, Roopan SM, Madhavi G, et al. Green chemical approach towards the synthesis of SnO2 NPs in argument with photocatalytic degradation of diazo dye and its kinetic studies. Journal of Photochemistry and Photobiology B: Biology. 2016, 162: 441-447.
https://doi.org/10.1016/j.jphotobiol.2016.07.010

[71] Chandran D, Nair LS, Balachandran S, et al. Structural, optical, photocatalytic, and antimicrobial activities of cobalt-doped tin oxide nanoparticles. Journal of Sol-Gel Science and Technology. 2015, 76(3): 582-591.
https://doi.org/10.1007/s10971-015-3808-z